A refined 3D reconstruction method for irregular ancient buildings

Xinting Zheng[1], Yansong Duan[1,*]

[1] School of Remote Sensing and Information Engineering, Wuhan University, Wuhan 430079, China
xintingzheng@whu.edu.cn; ysduan@whu.edu.cn

Commission II

Keywords: Irregular Ancient Architecture, Refined 3D Reconstruction, Unmanned Aerial Vehicles, Flight Path Planning.

Abstract

The refined three-dimensional (3D) reconstruction of ancient buildings using unmanned aerial vehicles (UAVs) is a crucial task in cultural heritage preservation. However, the complex structure, diverse shapes and non-regularity of ancient buildings make it difficult for traditional 3D reconstruction methods to fully cover all the details, resulting in poor quality reconstruction models. Therefore, this study proposes a novel 3D reconstruction method tailored for irregular ancient architecture, which adopts a "structural surface" guided strategy, and plans routes through the idea of "structural surfaces segmentation and then designing the routes", so as to obtain a high-resolution image set, and to ensure that the reconstruction model's fineness and completeness. Additionally, to tackle the slow speed and time-consuming nature of traditional modeling algorithms in establishing image adjacency relationships, this paper presents a method that utilizes flight path information to build these relationships. To validate the effectiveness of the proposed method, the Yellow Crane Tower in Wuhan, Hubei Province, China, was selected as a case study. Results indicate that the proposed method successfully enables the refined reconstruction of the Yellow Crane Tower, providing significant insights for the 3D reconstruction of irregular ancient buildings.

1. Introduction

Cultural heritage preservation has long been a global focus. As of 2023, 60 heritage sites have been listed as endangered, facing various potential threats such as natural disasters and armed conflicts. To enhance cultural heritage protection, the utilization of unmanned aerial vehicle (UAV) photogrammetry technology for refined three-dimensional reconstruction has gradually emerged as an effective approach (Higueras et al., 2021; Martínez-Carricondo et al., 2020; Ulvi, 2021). Ancient buildings, as significant components of cultural heritage, present considerable challenges for preservation efforts due to their complex structures and irregular shapes. Unlike ordinary buildings, ancient architecture typically features intricate designs and non-standard characteristics. Traditional methods for 3D reconstruction exhibit clear limitations when applied to such irregular ancient buildings. For instance, while three-dimensional laser scanning technology (He et al., 2022) can capture high-precision three-dimensional coordinates, the complexity and diversity of ancient structures can lead to shadowing and occlusion during scanning, resulting in data loss in these areas. Furthermore, laser scanning data often needs to be combined with photogrammetry data to generate a complete textured model, making it difficult to achieve this goal using laser scanning alone. Oblique photogrammetry techniques (Yang et al., 2022) reconstruct 3D models by capturing images from multiple angles, but conventional oblique photography strategies often fail to comprehensively cover all details due to the complex shapes and structures of ancient buildings, resulting in low-quality reconstructed models. In conclusion, the core problem of traditional 3D reconstruction lies in the existence of complex structural relationships of irregular ancient buildings, which prevent simple photography strategies from adequately capturing imagery; thus, there is a pressing need for improved photographic planning methods to determine optimal photographic locations and acquire comprehensive images of the structures.

Currently, significant research has been conducted by scholars on optimizing UAV photographic positions to achieve ideal imagery. For example, Kuang et al. (Kuang et al., 2020) designed initial paths based on scene top-down views, subsequently enhancing model quality through detailed close-ups. However, heuristic intelligent path planning technologies (Zhou et al., 2020) have increasingly replaced traditional path planning methods. These technologies seek to achieve an optimal balance between reconstruction results and minimal photographic costs through rational planning of shooting paths and viewpoints. Some researchers (Hepp et al., 2019; Koch et al., 2019) have adopted different optimization strategies based on initial three-dimensional models to select optimized subsets of viewpoints for final path planning. However, the optimized viewpoint sets derived from these viewpoint optimization techniques often struggle to conform to the complex surfaces of buildings, particularly in irregular structural regions. This limitation arises because these methods typically analyze the building as a whole rather than addressing the specific facade structures of the reconstruction object, thus failing to facilitate targeted path design for information collection. Li Qingquan et al. (Qingquan et al., 2022) proposed a Optimized Views Photogrammetry method integrating initial viewpoint generation and viewpoint optimization techniques for urban scene three-dimensional reconstruction. However, irregular ancient buildings differ from urban regular architectural clusters due to their complex shapes and structures, making the viewpoints computed by Optimized Views Photogrammetry suboptimal for irregular buildings. Zhang Zuxun et al. from Wuhan University (Zhang, 2019) proposed nap-of-the-object photogrammetry (NOOP) with a “from coarse to fine” flight path planning method, which can facilitate the three-dimensional reconstruction of various complex targets, providing insights for the reconstruction of irregular ancient architecture.

In terms of refined three-dimensional reconstruction, literature (Dai et al., 2021; Li et al., 2017) accomplishes façade element segmentation and extraction by effectively analyzing the building façade, so as to establish a high-quality 3D building model. However, these methods primarily focus on single facades, with

facade elements mostly consisting of regular geometric shapes such as windows and balconies. Literature (Bulatov et al., 2014; Han et al., 2022; Yan et al., 2017) extracted regular building facades based on original models or contour extraction and rooftop topology analysis, subsequently reconstructing each facade to improve three-dimensional model quality. However, for topologically complex irregular ancient buildings, the extraction of "regular facades" poses significant challenges. Nonetheless, the "surface-based" approach in these methods is of reference value for achieving refined modeling of irregular buildings.

Inspired by the aforementioned methods, this paper proposes a refined three-dimensional reconstruction approach for irregular ancient buildings, which takes “structural surface” as the unit, and adopts the idea of “structural surfaces segmentation and then designing the routes” to design a suitable route planning method for irregular buildings, thereby maximizing target coverage through a high-resolution image set to ensure the precision and integrity of the reconstructed model. Additionally, addressing the slow speed and time-consuming nature of traditional Structure-from-Motion (SFM) (Gao et al., 2022; Jiang et al., 2020; Patrucco et al., 2022) and Multi-View Stereo (MVS) (Masiero et al., 2019) techniques in establishing image adjacency relationships, this study presents a method for constructing an image adjacency graph using the planned flight path information.

The main contributions of this research can be summarized as follows: (1) A flight path planning method based on "Segmentation by structural surfaces and then designing the routes " tailored for irregular ancient buildings is proposed; (2) A method for obtaining image adjacency relationships based on flight path planning results, and then facilitating connection point matching, is introduced; (3) The above two points are employed to achieve the refined 3D reconstruction of the Yellow Crane Tower.

2. Methodology

The main process for the refined 3D reconstruction of irregular ancient buildings includes three key steps: obtaining a coarse point cloud model, planning photographic flight paths, and performing three-dimensional reconstruction. The processing flow is illustrated in Figure 1.

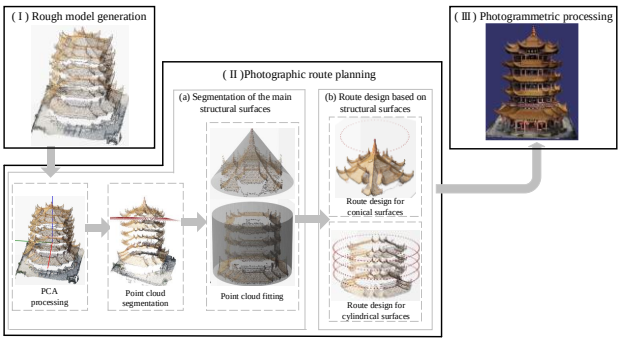

Figure 1. Workflow for the Refined 3D Reconstruction of Irregular Ancient Buildings

The process of obtaining a coarse point cloud model only requires using conventional methods to photograph the target and generate a sparse point cloud, which is a relatively mature technology and will not be discussed further in this paper. UAV photographic flight path planning and 3D reconstruction are crucial for addressing the refined modeling of irregular ancient buildings. The flight path planning consists of two subprocesses: main structure segmentation and flight path design based on structural surfaces. The key to improving the speed of 3D reconstruction is establishing image adjacency relationships.

2.1 Segmentation of the main structural surfaces

The objective of main structural surface segmentation is to divide irregular targets into smaller entities, which involves three primary steps: Principal Component Analysis (PCA), point cloud segmentation, and point cloud fitting.

(1) The fundamental principle of PCA is to transform the data through orthogonal transformation into a set of linear uncorrelated variables sorted by variance, preserving the main features and information of the data while reducing dimensionality (Yuan et al., 2016). Specifically, for any given target, the three principal directions are first determined, as shown in Figure 2(a). The resulting principal components PC_1, PC_2, and PC_3 represent the main geometric structural features of the irregular target..

(2) The purpose of point cloud segmentation is to segment the irregular target according to its geometric structural characteristics, yielding smaller targets with different geometric information. In this algorithm, the point cloud is first transformed into a new coordinate system where PC_2、PC_3、and PC_1 are designated as the X, Y, and Z axes, respectively. Subsequently, the target is segmented in the X, Y, and Z directions using a piecewise statistical method. The segmentation rule involves segmenting and statistically analyzing the distribution characteristics of projected points in each direction, designating areas of abrupt change as segmentation planes. The processing flow is illustrated in Figure 2(b), and the results are shown in Figure 2(c).

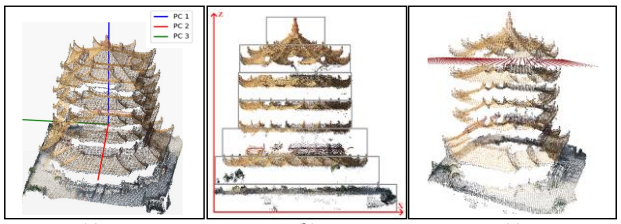

Figure 2. Point cloud segmentation. (a) PCA processing; (b)Piecewise statistical method for point cloud segmentation; (c) Point cloud segmentation results

(3) The objective of point cloud fitting is to provide a regularized description of the segmented point cloud. Common fitting surfac-

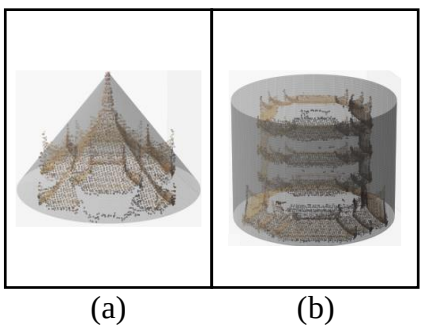

Figure 3. Regularized Fitting of Point Cloud. (a) Fitting using conical surface. (b) Fitting using cylindrical surface.

es include planes, cylindrical surfaces, and conical surfaces. In this study, an exhaustive search method is employed, where fitting is conducted using planes, cylindrical surfaces, and conical surfaces, retaining the type of fitting surface with the smallest error. Figure 3 shows the results of fitting using conical and cylindrical surfaces.

2.2 Flight path design based on structural surfaces

After main structure segmentation, multiple structural surfaces of the photographic target can be identified. At this point, corresponding flight path planning for each structural surface is necessary to design the most ideal photographic positions and orientations, enabling the acquisition of images that fully cover the photographic target. This paper primarily considers flight path design for three types of surfaces: planes, cylindrical surfaces, and conical surfaces. The flight path design for planes has been discussed in several articles, such as those by He Jianan et al. (He, 2019; Liu et al., 2022), and will not be further elaborated here. The focus will instead be on the flight path design for cylindrical and conical surfaces.

2.2.1 Flight Path Planning for Cylindrical Surfaces: The flight surface for cylindrical path planning is cylindrical in shape, with the UAV flying in a counterclockwise or clockwise direction around the target. Let the radius of the target be r and the flight distance be d, then the flight path radius R=r+d. All camera stations on the flight path must satisfy the following conditions: (1) Camera stations must be located within the flying cylindrical surface; (2) The distance between adjacent camera stations on the same flight path must be Δs; (3) The direction of the line connecting adjacent camera stations on the same flight path must be perpendicular to the main axis direction; (4) The distance between corresponding camera stations on adjacent flight paths must be Δh; (5) The line connecting corresponding camera stations on adjacent flight paths must be parallel to the central axis of the cylinder.

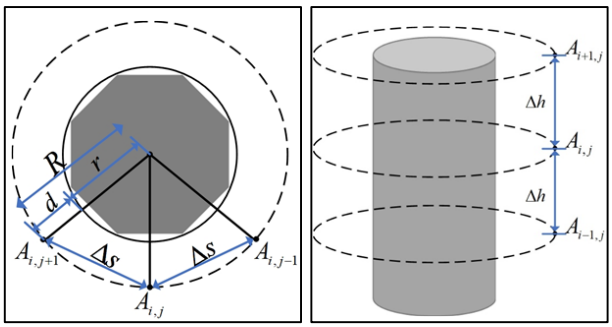

(a) (b)

Figure 4. Schematic Diagram of the Geometric Relationship Between Camera Stations on Cylindrical Flight Paths. (a) Illustrates the geometric relationship between adjacent camera stations on the same flight path; (b) Shows the geometric relationship between corresponding camera stations on adjacent flight paths.

Here, based on the distance Δs between adjacent camera stations on the same flight path and the flight radius R, the angular separation α between the two camera stations and the total number of camera stations n on a single flight path can be calculated. The calculation formulas are given in Equation (1). Additionally, using the flight path spacing Δh between two adjacent flight paths and the minimum flight height H_{min} and maximum flight height H, the number of flight paths μ can be computed, as shown in Equation (2).

$$\left.\begin{aligned} \alpha &= \sin^{-1}\frac{\Delta s}{2R} \\ n &= \frac{360^\circ}{\alpha} \end{aligned}\right\} \tag{1}$$

$$\mu = \frac{H - H_{min}}{\Delta h} \tag{2}$$

After designing multiple flight paths for cylindrical surfaces, it is essential to ensure there are no gaps between adjacent paths. This is achieved by tilting the camera's main optical axis at an angle γ both upward and downward at each position to create converging photography. For determining the tilt angle γ, as referenced in Figure 5, the tilted capture aligns the main optical axis with the center point of the images taken at adjacent camera stations in that tilt direction. This approach not only fulfills the task of image supplementation but also ensures that every point in the images meets the requirement for vertical three-fold overlap, providing favorable conditions for subsequent aerial triangulation and enhancing the accuracy of model reconstruction.

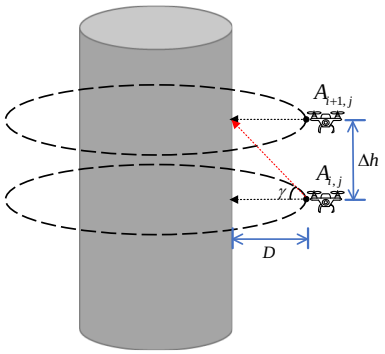

Figure 5. Schematic Diagram of Converging Photography in Cylindrical Flight Paths

Figure 5 illustrates the example of the main optical axis tilted upward. The black dashed lines represent the direction of the main optical axis perpendicular to the surface of the target at camera stations $A_{i,j}$ and $A_{i+1,j}$. The red dashed line indicates the direction of the main optical axis when tilted upward at camera station $A_{i,j}$.

2.2.2 Flight Path Planning for Conical Surfaces: For the conical flight path, a circular flight pattern is employed around the apex of the cone, while ensuring that the camera's main optical axis consistently aligns with the normal vector of the conical surface, pointing towards the midpoint of the cone's generatrix, as shown in Figure 6. By integrating the relevant parameters of the fitted cone, the circular flight path's radius R, relative flight height H, and camera tilt angle θ can be calculated under these conditions. Additionally, by controlling the number of circular captures, the actual distance between camera stations during flight can be determined, allowing for the acquisition of all camera station coordinates along the circular flight path, as well as the corresponding camera tilt angles at each station.

Considering that the reconstruction targets are structurally complex and rich in detail, converging photography is also introduced into the conical flight path to avoid occlusion and obtain more comprehensive three-dimensional information. At

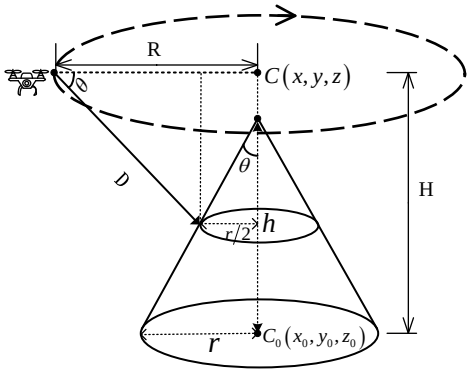

Figure 6. Schematic Diagram of the Geometric Relationship for Conical Flight Path

each camera station, the camera's main optical axis is tilted upward and downward at an angle γ. For determining the tilt angle γ, as referenced in Figure 7, an appropriate image overlap is set based on the relationship between the coverage of a single image and the size of the conical surface. The movement distance ΔS of the main optical axis along the direction of the cone's generatrix during tilted shooting is calculated, and combined with the photography object distance D to derive the tilt angle γ.

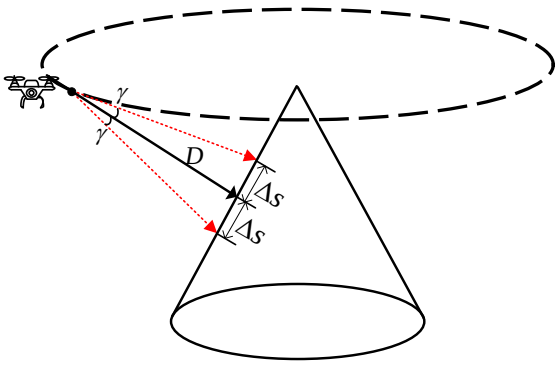

Figure 7. Schematic Diagram of Converging Photography in Conical Flight Paths

2.3 Establishment of Image Adjacency Relationships

Accurate image adjacency relationships can enhance the processing efficiency and quality of three-dimensional modeling. Based on the information from the drone flight paths, precise adjacency relationships can be established. In the flight path information, the coordinates of two images that are laterally adjacent satisfy Equation (3), while those that are vertically adjacent satisfy Equation (4).

$$\left.\begin{aligned}(x_i - x_j)^2 + (y_i - y_j)^2 &= \Delta s^2 \\ z_i &= z_j\end{aligned}\right\} \tag{3}$$

$$\left.\begin{aligned}z_i - z_j &= \Delta h \\ x_i &= x_j \\ y_i &= y_j\end{aligned}\right\} \tag{4}$$

In the equations, (x_i, y_i, z_i) and (x_j, y_j, z_j) represent the coordinates of two camera stations in the new coordinate system; Δs is the length of the photography baseline; and Δh is the interval between flight paths.

The image adjacency relationships obtained from the above algorithm are illustrated in Figure 8.

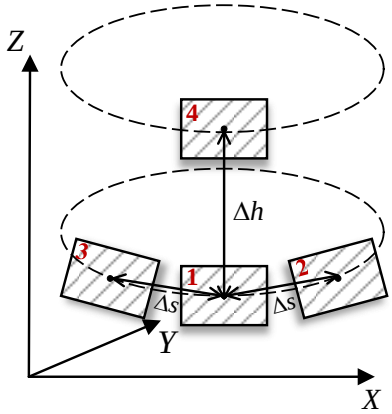

Figure 8. Schematic Diagram of Image Adjacency Relationships. Image 1 is laterally adjacent to Images 2 and 3, while Image 1 is vertically adjacent to Image 4.

In practical flights, due to factors such as GPS positioning errors and the instability of the drone, the actual locations of the camera stations can differ from the planned positions. When using Equations (3) and (4) for judgment, it is necessary to set a certain error threshold; as long as the differences fall within this threshold range, the conditions can be considered satisfied.

3. Experiments

3.1 Dataset

The experimental area selected for this study is the Yellow Crane Tower, located in Wuhan, Hubei Province, China. With a history of over 1,700 years, the Yellow Crane Tower is a renowned cultural landmark. Originally built during the Three Kingdoms period, it has been destroyed and rebuilt multiple times throughout history, with seven destructions and over ten reconstructions during the Ming and Qing dynasties alone. The current structure was rebuilt in 1985 and is situated atop Snake Mountain by the Yangtze River in Wuhan. As a typical example of Chinese pavilion architecture, the Yellow Crane Tower features a multi-layered stacked tower structure, consisting of five stories with a total height of 51.4 meters. The base measures 30 meters on each side, while the top layer measures 18 meters, with a maximum width of 32 meters. Each level is adorned with large murals, couplets, and cultural relics. The most notable characteristics of the Yellow Crane Tower are its irregular geometric structure and multiple upward-curving eaves design. This complex appearance and unique architectural structure present significant challenges for achieving detailed three-dimensional reconstruction of the tower.

Figure 9. Location Map of Yellow Crane Tower

Figure 10. Actual Image of Yellow Crane Tower

In this study, a DJI Phantom 4 RTK drone was used for photography, and the equipment details are provided in Table 1.

Focal length	8.8 mm
Field of view	84°
Image resolution	5472 x 3648
controllable rotation range,	pitch: -90° to +30°

Table 1. Relevant Information of DJI Phantom 4 RTK

To verify the effectiveness of the proposed method, we designed an experimental process that involves first segmenting the rough point cloud model of the Yellow Crane Tower using the main structure segmentation method, dividing it into smaller, more manageable targets. Next, we employ the structure-based flight path design method to plan the flight routes for each structural surface, ensuring complete coverage of the photographic target. After acquiring the image data, we utilize DPGrid software for the 3D modeling process, incorporating the drone flight path information during the image adjacency relationship establishment phase to enhance processing efficiency and quality. Finally, we conduct an analysis of the completeness and precision of the constructed refined 3D model of the Yellow Crane Tower.

3.2 Flight Path Planning

3.2.1 Main Structure Segmentation: Using the PCA algorithm, we processed the point cloud data of the Yellow Crane Tower to obtain the principal directions of the point cloud, clearly illustrating the 3D geometric features of the tower. The first principal component aligns with the vertical axis of the Yellow Crane Tower, reflecting the building's height. The second and third principal components correspond to the two main directions of the tower's cross-section, indicating its length and width characteristics in the horizontal plane. The processing results are shown in Figure 11.

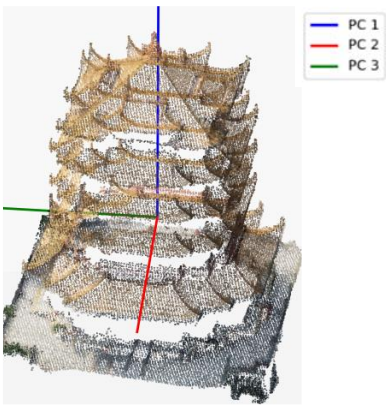

Figure 11. Principal Directions of the Yellow Crane Tower Point Cloud.The blue axis indicates the direction of the first principal component of the Yellow Crane Tower point cloud; the red axis represents the direction of the second principal component; the green axis shows the direction of the third principal component.

After performing point cloud segmentation and fitting, the main structure of the Yellow Crane Tower can be divided into two parts, A and B, as shown in Figure 12.

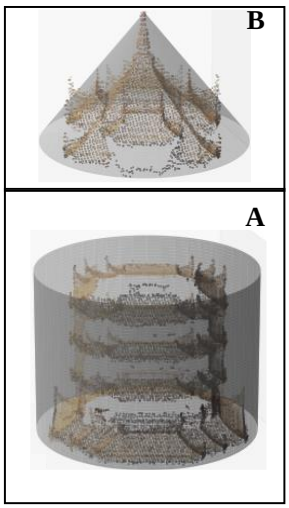

Figure 12. Segmentation Result of the Yellow Crane Tower Main Structure. The Yellow Crane Tower was divided into two parts, A and B

3.2.2 Cylindrical flight paths: To design the cylindrical flight paths for the main structure A of the Yellow Crane Tower, a cylinder with a fitted radius of $16m$ and a photography distance of $11m$ was used, resulting in a flight path radius of $27m$. The height of the cylindrical surface is $46m$. Given that the minimum safe flying height for the drone is $30m$, the starting height for the cylindrical paths was set at $30m$. In total, four flight paths were designed, each containing 85 camera stations, resulting in a total of 340 camera stations. The results are shown in Figure 13.

According to the requirements for convergent photography in the cylindrical flight paths, each point on the image must meet the condition of three-fold overlap in the vertical direction. At each camera station along the circular flight path, three shooting tasks were performed: one with the lens directed straight at the surface, one with the lens tilted upwards at an angle of 19.8°, and one with

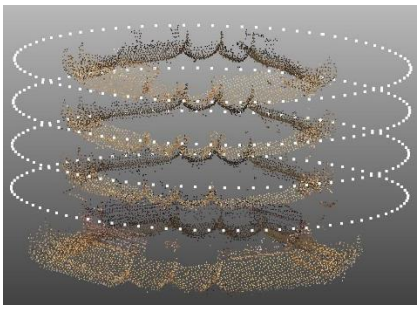

Figure 13. Illustrates the cylindrical flight paths for the Yellow Crane Tower.

the lens tilted downwards at the same angle. Ultimately, a total of 1,020 images were captured for the main structure A.

3.2.3 Conical flight path: For the main structure B of the Yellow Crane Tower, a conical flight path was designed. The radius of the conical base is 16 m, and the height of the cone is 5.5 m. Using the fitted data for the conical base radius and height, the camera tilt angle when the optical axis is directed towards the cone's generatrix was calculated to be 71°.

Considering image resolution and coverage, the ground sampling distance (GSD) for the circular flight path was set to 3.2 mm/pixel, resulting in a corresponding photography distance $D = 11.7m$. To ensure adequate image overlap, the distance between adjacent camera stations on the circular flight path was set to 1.5 m. During convergent photography at the same camera station, the optical axis was tilted upwards and downwards at an angle of 14.4°.

The planned conical flight path has a surrounding flight radius of 11.8 m, with a relative flight height of 13.78 m from the segmentation plane. The number of surrounding captures was controlled to 50, resulting in a total of 150 images captured for the main structure B. The results of the conical flight path are shown in Figure 14.

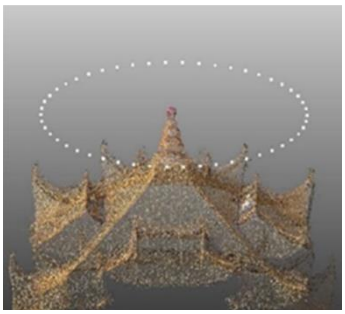

Figure 14. Schematic of the conical flight path for the Yellow Crane Tower.

3.3 Photogrametry Processing

Based on the results of the cylindrical flight path planning, close-up images of the main structure of the Yellow Crane Tower were obtained. Additionally, close-up images of the top of the tower were captured following the conical flight path planning. Close-range images of areas below 30 meters in height were acquired using handheld photography.

After completing the image acquisition tasks, the high-resolution, high-overlap images were processed using DPGrid software for subsequent photogrammetric processing. Initially, the flight path planning information was used to establish the adjacency relationships between the imported images, thereby accelerating processing speed. Ultimately, a refined three-dimensional model of the Yellow Crane Tower was constructed.

3.4 Results and Analysis

Figures 15-18 show the four main sides of the refined 3D model of the Yellow Crane Tower, as well as detailed images corresponding to these sides. Figures 15(a), 16(a), 17(a), and 18(a) depict the overall model of the four main sides. The reconstructed 3D model of the Yellow Crane Tower faithfully reproduces the real appearance of the tower, and the dimensions of the model maintain a proportional scale relationship with the actual structure in terms of length, width, and height. Figures 15(b), 16(b), 17(b), and 18(b) show the detailed reconstruction of the plaques hanging on the four main sides. The model demonstrates high precision in reconstructing the plaques and the characters on them. The strokes are smooth, and the characters are accurately shaped and clearly legible. Figure 15(c) displays the reconstruction result of the mural on the northern wall. The model not only retains the mural's texture and line details with precision but also faithfully reproduces its color information, making the reconstruction realistic. Figure 16(c) shows an eave structure on the eastern side. The upturned eaves are not only structurally complex but also rich in texture. The reconstructed model achieves a highly accurate reproduction of this unique structure, capturing both its geometric features and the intricate wood carvings on the eaves. Figure 17(c) presents the reconstruction of a railing structure on the southern side, demonstrating excellent clarity in the reconstruction of this part with hollowed-out structures, maintaining clear boundaries and high precision. Figure 18(c) shows the detailed reconstruction of windows on the western side. The model accurately restores the texture details of the decorative elements on the window frames and clearly presents the reflective properties of the window glass.

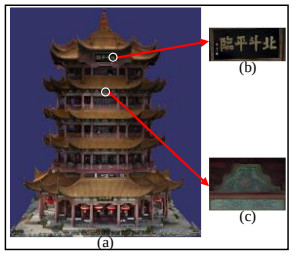

Figure 15. North of the model

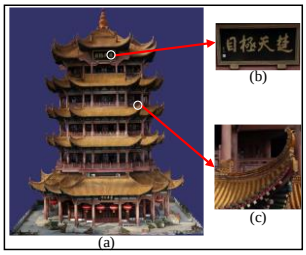

Figure 16. East of the model

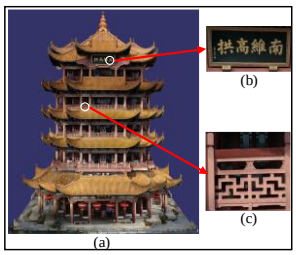

Figure 17. South of the model

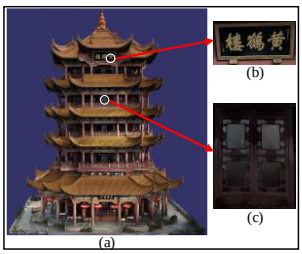

Figure 18. West of the model

For this irregular ancient building, the refined 3D model achieved in this study ensures both geometric and texture completeness and realism. It not only provides a clear and comprehensive representation of the building's complex appearance and unique architectural features but also captures fine details with high accuracy.

4. Conclusion

The complex structural characteristics of irregular ancient buildings pose significant challenges for refined 3D reconstruction. Traditional photogrammetry methods and flight path planning exhibit clear limitations, making the rational design of photographic flight paths a key issue for achieving refined 3D reconstruction. This paper proposes a flight path planning method for refined 3D reconstruction of irregular ancient architecture, employing the idea of " structural surfaces segmentation and then designing the routes " to create flight paths that better conform to building surfaces, resulting in a wide coverage and high-resolution image set. Taking the Yellow

Crane Tower as a case study, PCA was utilized to complete the " structural surface segmentation," and designed " cylindrical flight paths and conical flight paths" as the photographic route planning results. The clear positional relationships among images obtained along the planned paths allowed for research into a rapid 3D reconstruction method guided by flight path positioning, leveraging pose information to establish adjacency relationships between images. The results indicate that the " structural surface segmentation"-based flight path planning method significantly enhances the reconstruction quality of irregular buildings, accurately reflecting the rich texture details and complete architectural structure.

Combining the flexibility and powerful data collection capabilities of drones, the "structural surface segmentation"-based flight path planning method shows great potential for promotion and application in the refined 3D reconstruction and preservation of irregular ancient architecture. While the flight path planning results designed for the Yellow Crane Tower in this study demonstrate good effectiveness for this specific building, they may not be directly applicable to structures with different architectural characteristics. Additionally, during actual photography, the continuous adjustment of drone flight posture and shooting angles will inevitably lead to increased time consumption. Therefore, future research will further explore ways to enhance the universality, efficiency, and energy consumption of flight path planning results.

Acknowledgements

This study was supported by National Key Research and Development Program of China, No. 2023YFB3905704.

References

Bulatov, D., Häufel, G., Meidow, J., Pohl, M., Solbrig, P., Wernerus, P., 2014. Context-based automatic reconstruction and texturing of 3D urban terrain for quick-response tasks. ISPRS Journal of Photogrammetry and Remote Sensing 93, 157–170. https://doi.org/10.1016/j.isprsjprs.2014.02.016

Dai, M., Ward, W.O.C., Meyers, G., Densley Tingley, D., Mayfield, M., 2021. Residential building facade segmentation in the urban environment. Building and Environment 199, 107921. https://doi.org/10.1016/j.buildenv.2021.107921

Gao, L., Zhao, Y., Han, J., Liu, H., 2022. Research on Multi-View 3D Reconstruction Technology Based on SFM. Sensors 22, 4366. https://doi.org/10.3390/s22124366

Han, Y., Zhou, S., Xia, P., Zhao, Q., 2022. Research on fine 3D modeling technology of tall buildings based on UAV Photogrammetry, in: 2022 3rd International Conference on Geology, Mapping and Remote Sensing (ICGMRS). Presented at the 2022 3rd International Conference on Geology, Mapping and Remote Sensing (ICGMRS), IEEE, Zhoushan, China, pp. 349–353. https://doi.org/10.1109/ICGMRS55602.2022.9849357

He, J., 2019. Nap-of-the-Object Photogrammetry and Its Key Techniques, Wuhan University. 10.27379/d.cnki.gwhdu.2019.000509

He, K., Sui, C., Huang, T., Dai, R., Lyu, C., Liu, Y.-H., 2022. 3D Surface reconstruction of transparent objects using laser scanning with LTFtF method. Optics and Lasers in Engineering 148, 106774. https://doi.org/10.1016/j.optlaseng.2021.106774

Hepp, B., Nießner, M., Hilliges, O., 2019. Plan3D: Viewpoint and Trajectory Optimization for Aerial Multi-View Stereo Reconstruction. ACM Trans. Graph. 38, 1–17. https://doi.org/10.1145/3233794

Higueras, M., Calero, A.I., Collado-Montero, F.J., 2021. Digital 3D modeling using photogrammetry and 3D printing applied to the restoration of a Hispano-Roman architectural ornament. Digital Applications in Archaeology and Cultural Heritage 20, e00179. https://doi.org/10.1016/j.daach.2021.e00179

Jiang, S., Jiang, C., Jiang, W., 2020. Efficient structure from motion for large-scale UAV images: A review and a comparison of SfM tools. ISPRS Journal of Photogrammetry and Remote Sensing 167, 230–251. https://doi.org/10.1016/j.isprsjprs.2020.04.016

Koch, T., Körner, M., Fraundorfer, F., 2019. Automatic and Semantically-Aware 3D UAV Flight Planning for Image-Based 3D Reconstruction. Remote Sensing 11, 1550. https://doi.org/10.3390/rs11131550

Kuang, Q., Wu, J., Pan, J., Zhou, B., 2020. Real-Time UAV Path Planning for Autonomous Urban Scene Reconstruction, in: 2020 IEEE International Conference on Robotics and Automation (ICRA). Presented at the 2020 IEEE International Conference on Robotics and Automation (ICRA), IEEE, Paris, France, pp. 1156–1162. https://doi.org/10.1109/ICRA40945.2020.9196558

Li, Z., Zhang, Liqiang, Mathiopoulos, P.T., Liu, F., Zhang, Liang, Li, S., Liu, H., 2017. A hierarchical methodology for urban facade parsing from TLS point clouds. ISPRS Journal of Photogrammetry and Remote Sensing 123, 75–93. https://doi.org/10.1016/j.isprsjprs.2016.11.008

Liu, X., Ji, Z., Zhou, H., Zhang, Z., Tao, P., Xi, K., Chen, L., Marcato Junior, J., 2022. An object-oriented UAV 3D path planning method applied in cultural heritage documentation. ISPRS Ann. Photogramm. Remote Sens. Spatial Inf. Sci. V-1–2022, 33–40. https://doi.org/10.5194/isprs-annals-V-1-2022-33-2022

Martínez-Carricondo, P., Carvajal-Ramírez, F., Yero-Paneque, L., Agüera-Vega, F., 2020. Combination of nadiral and oblique UAV photogrammetry and HBIM for the virtual reconstruction of cultural heritage. Case study of Cortijo del Fraile in Níjar, Almería (Spain). Building Research & Information 48, 140–159. https://doi.org/10.1080/09613218.2019.1626213

Masiero, A., Chiabrando, F., Lingua, A.M., Marino, B.G., Fissore, F., Guarnieri, A., Vettore, A., 2019. 3D Modeling of girifalco fortress. Int. Arch. Photogramm. Remote Sens. Spatial Inf. Sci. XLII-2/W9, 473–478. https://doi.org/10.5194/isprs-archives-XLII-2-W9-473-2019

Patrucco, G., Giulio Tonolo, F., Sammartano, G., Spanò, A., 2022. SFM-Based 3D reconstruction of heritage assets using UAV thermal images. Int. Arch. Photogramm. Remote Sens. Spatial Inf. Sci. XLIII-B1-2022, 399–406. https://doi.org/10.5194/isprs-archives-XLIII-B1-2022-399-2022

Qingquan, L.I., Hui, H., San, J., Qingwu, H.U., Wenshuai, Y.U., 2022. Optimized views photogrammetry and its precision analysis. Acta Geodaetica et Cartographica Sinica 51, 996. https://doi.org/10.11947/j.AGCS.2022.20210685

Ulvi, A., 2021. Documentation, Three-Dimensional (3D) Modelling and visualization of cultural heritage by using Unmanned Aerial Vehicle (UAV) photogrammetry and terrestrial laser scanners. International Journal of Remote Sensing 42, 1994–2021. https://doi.org/10.1080/01431161.2020.1834164

Yan, Y., Gao, F., Deng, S., Su, N., 2017. A Hierarchical Building Segmentation in Digital Surface Models for 3D Reconstruction. Sensors 17, 222. https://doi.org/10.3390/s17020222

Yang, B., Ali, F., Zhou, B., Li, S., Yu, Y., Yang, T., Liu, X., Liang, Z., Zhang, K., 2022. A novel approach of efficient 3D reconstruction for real scene using unmanned aerial vehicle oblique photogrammetry with five cameras. Computers and Electrical Engineering 99, 107804. https://doi.org/10.1016/j.compeleceng.2022.107804

Yuan, C., Yu, X., Luo, Z., 2016. 3D point cloud matching based on principal component analysis and iterative closest point algorithm, in: 2016 International Conference on Audio, Language and Image Processing (ICALIP). Presented at the 2016 International Conference on Audio, Language and Image Processing (ICALIP), IEEE, Shanghai, China, pp. 404–408. https://doi.org/10.1109/ICALIP.2016.7846655

Zhang, Z., 2019. Origin and Meaning of Nap-of-the-Object Photogrammetry (Research Report). Wuhan University, Wuhan.

Zhou, X., Xie, K., Huang, K., Liu, Y., Zhou, Y., Gong, M., Huang, H., 2020. Offsite aerial path planning for efficient urban scene reconstruction. ACM Trans. Graph. 39, 1–16. https://doi.org/10.1145/3414685.3417791